DOI: 10.1002/anie.201002711

Diffusion in Nanochannels

Anomalous Diffusion of Electrically Neutral Molecules in Charged Nanochannels**

Wei Chen, Zeng-Qiang Wu, Xing-Hua Xia, Jing-Juan Xu, and Hong-Yuan Chen*

Diffusion is the principal means of passive transport whereby ions or molecules driven by thermal motion move along their concentration gradients. This spontaneous process is widespread in nature. For example, as the main form of transport for vital materials through cell membranes, diffusion plays a fundamental role in living cells. Recently, self-supporting membranes that contain single or arrays of nanochannels are attracting increasing attention in nanotechnology, chemistry, physics, and biology.[1–5] Inspired by biological membrane channel systems, most notably the α-hemolysin channel,[6,7] artificial analogues of such nanoscopically sized pores have been developed for potential application in controlled growth of nanostructures, nanofiltration devices, bioseparation, and biosensing.[8–14] Compared to biologically based nanochannels, artificial inorganic nanochannels have potential advantages of being less fragile, more stable, easily tailored, and flexible with regard to surface modification. Anodization of aluminum under appropriate electrochemical conditions yields extended membranes containing self-assembled, uniform, parallel pores with diameters of a few tens to a few hundreds of nanometers, high pore density, and well-defined morphology.[15–19] Such porous anodic alumina (PAA) membranes could find applications in chemical and biological separations as well as for analytical purposes.[20,21] Motion of molecules across these charged membranes is the basis of numerous systems of technological and biological interest. Detailed knowledge of such mass-transport behavior is therefore crucial for understanding and optimizing prospective device structures. Although many application models have been successfully established on the basis of the widely studied migration mechanism of ions or charged biomolecules in nanochannels,[22–29] little is known about the motion of electrically neutral molecules on this size scale. Herein we show a distinct diffusion phenomenon of electrically neutral molecules in charged alumina nanochannels.

Mass transfer across a porous membrane is governed by the Nernst–Planck equation. For a one-dimensional system, the mass transfer J along the x axis can be written as Equation (1) where D, C, and z are the diffusion coefficient,

$$J(x) = -D\frac{\partial C(x)}{\partial x} - \frac{zF}{RT}DC\frac{\partial \phi(x)}{\partial x} + Cv_{eo}(x) \quad (1)$$

concentration, and charge of the permeating species, respectively, $\partial C(x)/\partial x$ is the concentration gradient at distance x, $\partial \phi(x)/\partial x$ the potential gradient, and v_{eo} the electroosmotic velocity.

The three terms on the right-hand side of Equation (1) represent the contribution of 1) diffusion, which moves both charged and electrically neutral species under the influence of a concentration gradient, 2) electromigration, which moves charged species toward the oppositely charged electrode, and 3) electroosmotic flow, which is driven by the mobile double layer of the inner pore wall and moves the entire liquid along one direction under the influence of an electric field gradient. Among these three mass-transport processes, diffusion is inevitable. In the absence of an electrical driving force, only the first term on the right-hand side of Equation (1) is operative and the flux through the porous membrane is purely due to diffusion, which is only proportional to the concentration gradient according to Fick's law.

However, we have now found for the first time a distinct diffusion phenomenon in 20 nm alumina nanochannels. The alumina nanochannels used here were fabricated in sulfuric acid by a two-step method involving anodization and electrochemical detachment.[30,31] The diffusion flux of phenol, a neutral molecule commomly used as indicator in studies of mass-transport behavior in nanochannels,[32] varies with the ionic strength in such porous anodic alumina nanochannels. This anomalous non-Fickian behavior can be mainly attributed to restricted diffusion of polar molecules in the electric double layer (EDL), a shielding layer that is created near a charged surface in contact with an electrolyte. Polarization of electrons in p or π orbitals by a strong surface electric field reportedly plays an important role in the interaction between the aromatic molecules and the alumina surface.[33] In the present case, the electrons of the hydroxyl group of phenol are polarized by the charged alumina surface, and this results in the formation of an inductive dipole which interacts with the alumina surface. This interaction decreases the diffusion flux of phenol in the EDL and can be used to explain the observed anomalous non-Fickian behavior in nanochannels.

[*] Dr. W. Chen,[+] Dr. Z. Q. Wu, Prof. X. H. Xia, Prof. J. J. Xu, Prof. H. Y. Chen
Key Laboratory of Analytical Chemistry for Life Science
School of Chemistry and Chemical Engineering, Nanjing University
Nanjing 210093 (China)
E-mail: xhxia@nju.edu.cn

[+] Permanent address: Department of Pharmaceutical Analysis, School of Pharmacy, Fujian Medical University
Fuzhou 350004 (China)

[**] This work was financially supported by the National Basic Research Program (2007CB714501, 2007CB936404), the National Natural Science Foundation of China (21035002, 20828006, 20890020, 20975047), and the National Science Fund for Creative Research Groups (20821063).

Supporting information for this article is available on the WWW under http://dx.doi.org/10.1002/anie.201002711.

The model of restricted diffusion across an alumina nanochannel is illustrated in Figure 1. When alumina, an amphoteric material, is in contact with an aqueous solution, its surface is hydrolyzed to form AlOH surface groups, which

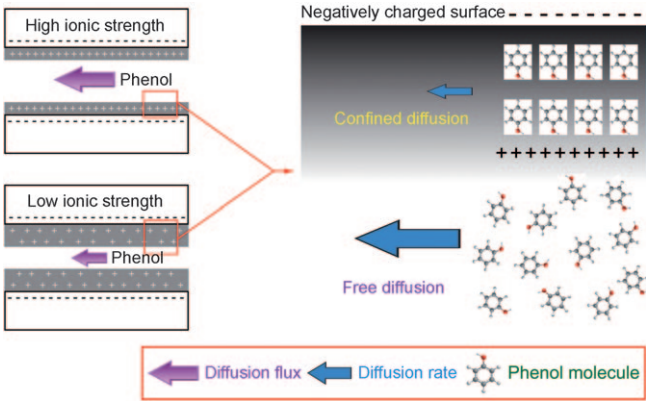

Figure 1. Diffusion of phenol molecules across charged alumina nanochannels.

can be positively charged ($AlOH_2^+$), neutral (AlOH), or negatively charged (AlO^-), depending on the pH of the electrolyte solution.[34] Under the pH conditions in our study, the channel surface is negatively charged and attracts positive ions, while negative ions are repelled, keeping the bulk of the liquid electrically neutral.

Diffusion of phenol molecules through the PAA nanochannels can be divided into two distinctively different contributions: free diffusion in the region outside the EDL, and confined diffusion inside the EDL. As discussed above, the diffusion flux of phenol in the EDL is decreased due to the interaction between the inductive dipole of phenol and the PAA surface. Thus, the total diffusion flux of phenol in nanochannels varies with the EDL thickness. However, this effect is negligible in the free-diffusion region outside the EDL. For simplicity, it is assumed that the motion of phenol molecules in the free-diffusion region is similar to that in bulk systems.

The spatial distribution of confined- and free-diffusion regions depends on the thickness of the EDL, which is determined by the ionic strength of the electrolyte. The extent of the EDL can be approximately predicted by the Debye length λ_D, which depends on the molar concentration of the ionized fluid, and its thickness λ_D can be estimated by means of the Debye–Hückel parameter κ [Eq. (2)] where n is the concentration, k_B the Boltzmann constant, e the electron charge, z the valence, T the absolute temperature, ε_0 the dielectric permittivity of vacuum, and ε the dielectric constant of the solvent.

$$\kappa = \frac{1}{\lambda_D} = \sqrt{\frac{e^2 \sum_i n_i z_i^2}{\varepsilon \varepsilon_0 k_B T}} \qquad (2)$$

In the case of high ionic strength, the confined-diffusion region shrinks, while the free-diffusion region expands. On the contrary, the confined-diffusion region expands while the free-diffusion region shrinks in the case of low ionic strength. As a result, the diffusion flux is expected to increase with increasing ionic strength of the electrolytes.

Figure 2a shows the distinct diffusion behavior of phenol through 20 nm alumina nanochannels in phosphate-buffered saline (PBS) at different pH values in the range of 6.0–8.0. The variation of the diffusion flux with the ionic strength of the electrolyte is almost the same. However, lower diffusion flux was observed at higher pH values. This difference can be explained by the enhanced confinement of motion in the EDL due to the increased surface charge density at higher pH values, which enhances the interaction between the electric field and phenol molecules.

The restricted-diffusion model can also be used to explain the different diffusion flux observed in different buffer systems. Under the same conditions, the diffusion flux in Tris-HCl (Tris = tris(hydroxymethyl)aminomethane) buffer solution is larger than in PBS (Figure 2d). As demonstrated in our previous work, specific adsorption of anions on the alumina surface plays an important role in the electric property of the nanochannels. The specific adsorption of anions on the internal walls of the alumina nanochannels produces a more negatively charged surface. It has been proposed that the adsorbability of the phosphate anion is greater than that of the chloride anion.[34] This can be confirmed by the different shifts of the isoelectric point of alumina nanochannels in PBS and Tris-HCl buffer (Figure 2e). In PBS, the apparent isoelectric point shifts to a more acidic pH because increased H^+ adsorption is necessary to neutralize more negative charges of the adsorbed phosphate anions.

As the spatial contribution of the confined- and free-diffusion regions plays an important role in diffusion of phenol across the nanochannels, the pore-size effect was investigated by using PAA membranes with different pore diameters. First, a self-supporting PAA membrane with 40 nm pore diameter was fabricated in oxalic acid electrolyte by anodization and electrochemical detachment. Although the confined-diffusion phenomenon also exists in this case, the ionic strength has less influence on the diffusion flux (Figure 3a). The smaller diffusion flux observed in 40 nm nanochannels compared to 20 nm nanochannels can be attributed to the following factors: 1) the thickness of the membrane with 40 nm nanochannels of 33.5 μm is greater than that of the membrane with 20 nm nanochannels (17.5 μm; Figure S1, Supporting Information); 2) the pore opening on the bottom side of the membrane with 40 nm nanochannels is about 20 nm (Figure 3c). Together with the smaller pore density of this membrane, the real pore area in contact with solution at the bottom side is about one-fourth of that with 20 nm pores (measured from Figure 2c and 3c). Further evidence of a pore-size effect is revealed by the almost constant diffusion flux across an alumina membrane with 200 nm pores (Figure 3d).

This pore-size effect can be elucidated by means of the double-layer thickness and its percentage of the pore cross section under various conditions. The charge density and potential within the nanochannel can be formulated by the

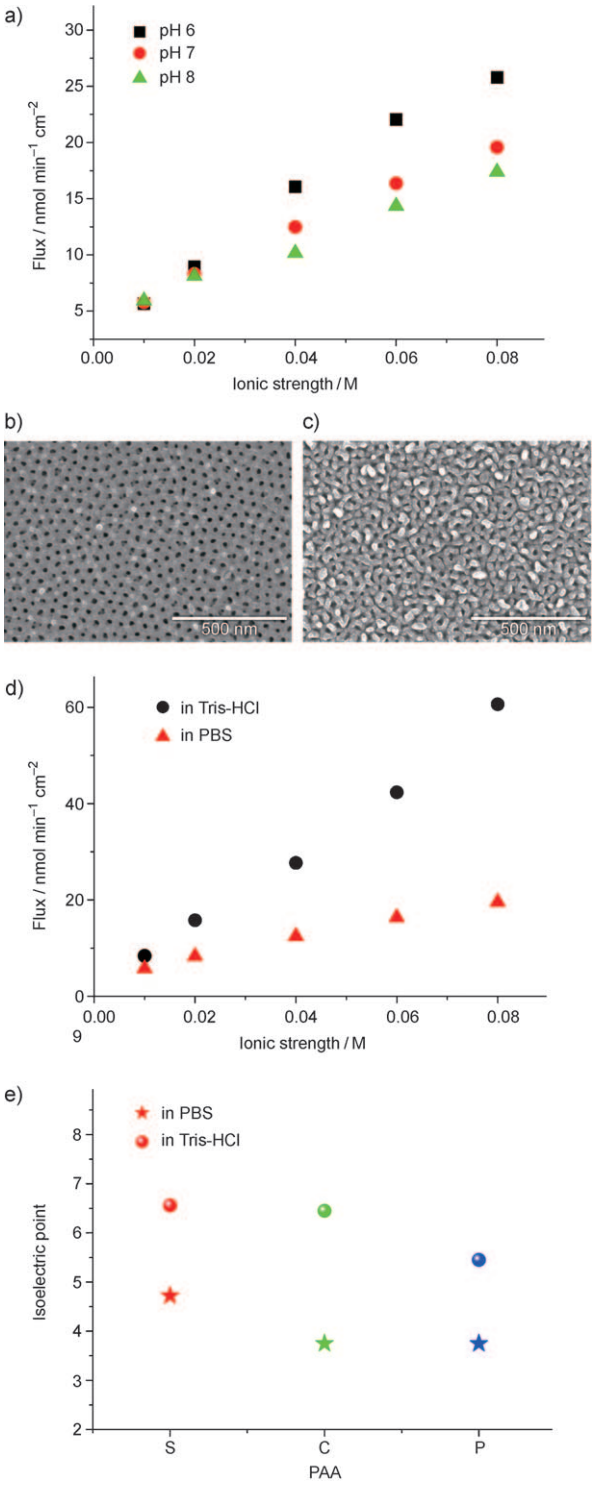

Figure 2. Influence of ionic strength on the diffusion flux. a) Plots of diffusion flux versus ionic strength in PBS, pH 6.0, 7.0, and 8.0. scanning electron microscopy (SEM) images of the top surface (b) and bottom surface (c) of a highly ordered porous anodic alumina membrane prepared by anodizing a aluminum sheet at 20 V in 0.2 M H_2SO_4 for 1 h in the first step and 4 h in the second step. d) Plots of diffusion flux versus ionic strength in PBS and Tis-HCl buffer solution, pH 7.0. e) Isoelectric point of the porous anodic alumina in PBS and Tris-HCl buffer solution. S, C, and P represent PAA fabricated in sulfuric acid, oxalic acid, and phosphoric acid electrolytes, respectively.

Poisson equation in cylindrical coordinates [Eq. (3)] where $\rho(r)$ is the net charge density at distance r from the axis, ε the dielectric constant, and ψ the potential at distance r from the axis.

$$\frac{1}{r}\frac{d}{dr}\left(r\frac{d\psi}{dr}\right) = -\frac{\rho(r)}{\varepsilon} \tag{3}$$

For a symmetric univalent electrolyte in the buffer, the charge density is given by Equation (4) where n is the Avogadro constant, e the electron charge, c the concentration of the buffer, and z the valence of ions. Since the concentration of ions at distance r from the axis conforms to the Boltzmann distribution, Equation (4) can be further developed as Equation (5) where c_0 is the bulk concentration of the buffer. The Poisson–Boltzmann equation for nanochannels was built by taking Equation (5) into Equation (3) [Eq. (6)].

$$\rho(r) = ne\sum_i z_i c_i \tag{4}$$

$$\rho(r) = -nec_0\left[\exp\left(\frac{-e\psi}{k_B T}\right) - \exp\left(\frac{e\psi}{k_B T}\right)\right] = -2nec_0\sinh\left(\frac{e\psi}{k_B T}\right) \tag{5}$$

$$\frac{1}{r}\frac{d}{dr}\left(r\frac{d\psi}{dr}\right) = \frac{2nec_0}{\varepsilon}\sinh\left(\frac{e\psi}{k_B T}\right) \tag{6}$$

When $e\psi/k_B T$ is small, the function $\sinh(e\psi/k_B T) \approx e\psi/k_B T$. Based on this assumption, Equation (6) can be simplified to Equation (7). Based on reference [35] the Equation (7) then becomes Equation (8) where $k = (2ne^2c_0/\varepsilon k_B T)^{1/2}$ is the reciprocal of the double-layer thickness. According to this formulation, the double-layer thickness of nanochannels of different sizes is calculated.

$$\frac{1}{r}\frac{d}{dr}\left(r\frac{d\psi}{dr}\right) = \frac{2ne^2c_0}{\varepsilon k_B T}\psi \tag{7}$$

$$\frac{1}{r}\frac{d}{dr}\left(r\frac{d\psi}{dr}\right) = k^2\psi \tag{8}$$

To verify the double-layer thicknesses calculated with the approximate Equation (8), numerical solutions of Equation (6) were calculated by using the finite-element method. It has been reported that when ψ_0 is smaller than 50 mV, the results of the approximation are in good agreement with the exact solutions.[35] In our finite-element calculation, ψ_0 was also set to 50 mV, and the numerical solutions to the double-layer thickness (see Supporting Information) are indeed in good agreement with those obtained from the approximate treatment.

Table 1 lists the calculated results under various conditions in Tris-HCl buffer solution. Compared to the 20 nm pores, the free-diffusion region is much larger than the confined-diffusion region in 200 nm pores. Therefore, the influence of the spatial variation of the confined-diffusion region with the ionic strength on the diffusion flux can be reasonably neglected.

In summary, the interaction between the electric field and phenol molecules restricts the self-diffusion of these electrically neutral polar molecules in the EDL. The total diffusion

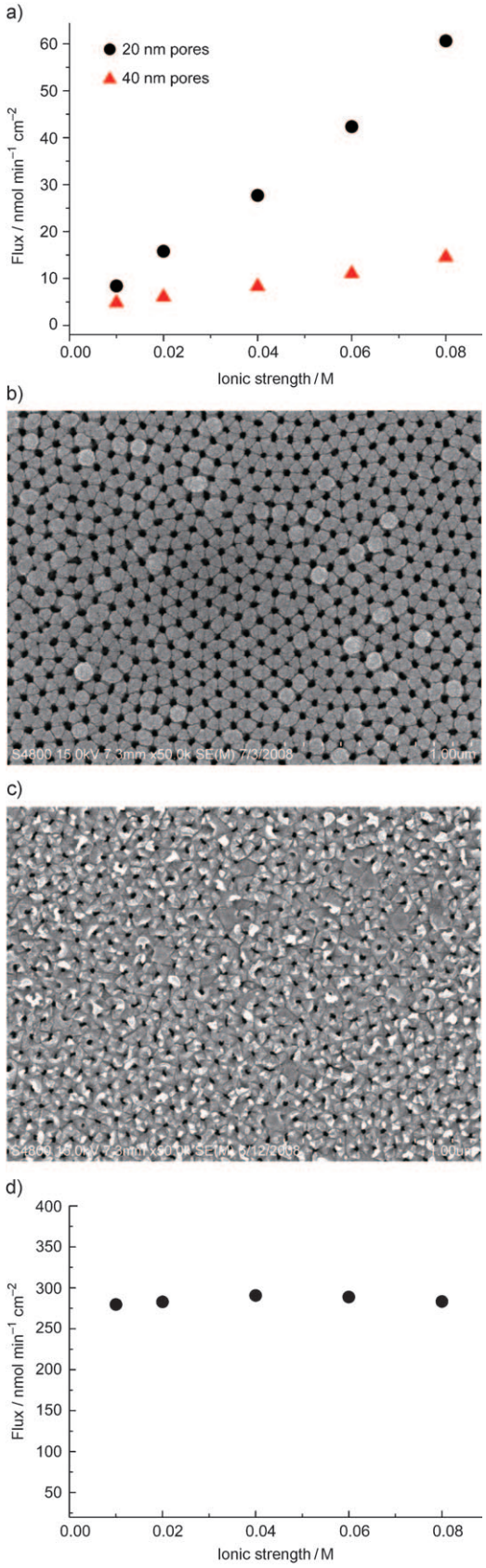

Table 1: Double-layer thickness and its percentage of the pore cross section under different conditions.

c [mM]	20 nm pore		200 nm pore	
	κ^{-1} [nm]	% pore cross-section	κ^{-1} [nm]	% pore cross-section
10	3.04	51.56	3.04	5.99
20	2.15	38.38	2.15	4.25
40	1.52	28.09	1.52	3.02
60	1.24	23.26	1.24	2.46
80	1.07	20.26	1.07	2.13

flux across the nanochannels is determined by the spatial distribution of the confined- and free-diffusion regions. The ionic strength of the electrolyte and the pore surface charge density play important roles in determining the diffusion flux. The contribution of the confined-diffusion region to the total diffusion flux strongly depends on the pore size. These findings on the anomalous non-Fickian behavior of polar molecules in charged nanochannels may be helpful in the development of nanofluidic devices. In addition, potential applications may lie in the unique state and properties of molecules confined by the electric field in nanochannels.

Experimental Section

Preparation of PAA membranes: Ordered porous alumina membranes were prepared by a two-step process of anodization and electrochemical detachment, described in detail in our previous work.[30,31] Briefly, the anodization was carried out with a two-electrode configuration at constant voltage from a vigorously stirred solution of sulfuric acid or oxalic acid under thermostatic conditions. The aluminum sheet was first anodized for 1 h, and then it was immersed in an aqueous solution of phosphochromic acid (6% H_3PO_4 + 1.8% H_2CrO_4) at 60 °C with ultrasonication for 30 min to remove the preformed PAA film and leave the aluminum base intact, followed by multiple rinsing with distilled water. After the alumina film was stripped off, the sample was oxidized for 4 h under the same conditions as described in the first step. To obtain a free-standing through-hole membrane, the sample was anodically oxidized in a solution of $HClO_4$ (72 wt%) and CH_3CH_2OH (1:1 v/v) at a voltage 10 V higher than its formation voltage for 3 s. After this process, the porous alumina film separated from the barrier layer immediately. The free-standing PAA membrane was then rinsed in double-distilled water. The surface morphologies of the PAA membranes were characterized with a JSM-6360 LV scanning electron microscope.

Mass-transport experiment: The experimental setup is schematically depicted in Figure S3 of the Supporting Information. The membrane was clamped between plastic films and then placed between the two halves of cells. Prior to the experiment, the membranes were left for at least 1 h in the buffer solution to ensure

Figure 3. Pore-size effect. a) Plots of diffusion flux versus ionic strength in Tris-HCl buffer solution (pH 7.0). PAA was fabricated in 0.2 M H_2SO_4 at 20 V (pore diameter: 20 nm) and in 0.3 M $H_2C_2O_4$ at 40 V (pore diameter: 40 nm). SEM images of the top surface (b) and bottom surface (c) of a highly ordered porous anodic alumina membrane prepared by anodizing an aluminum sheet at 40 V in 0.3 M $H_2C_2O_4$ for 1 h in the first step and 4 h in the second step. d) Plots of diffusion flow versus ionic strength in Tris-HCl buffer solution (pH 7.0). PAA (Whatman) with 200 nm pore diameter was used.

complete wetting. Mass-transport experiments were carried out by adding 5.0 mL of 50 mM phenol to the feed half-cell and 5.0 mL buffer solution to the permeation half-cell. The diffusion flux was determined by monitoring the concentration change of phenol at the permeation half-cell. This was accomplished by UV detection of the permeation solution with a UV/Vis spectrophotometer (UV-2401 PC, Shimadzu) at 270 nm. The absorbance data were converted to moles of phenol transported with the aid of a calibration curve.

Received: May 5, 2010
Revised: July 28, 2010
Published online: September 15, 2010

Keywords: diffusion · membranes · mesoporous materials · nanostructures · porous anodic alumina

[1] H. Bayley, C. R. Martin, *Chem. Rev.* **2000**, *100*, 2575 – 2594.
[2] D. W. Deamer, D. Branton, *Acc. Chem. Res.* **2002**, *35*, 817 – 825.
[3] R. J. White, E. N. Ervin, T. Yang, X. Chen, S. Daniel, P. S. Cremer, H. S. White, *J. Am. Chem. Soc.* **2007**, *129*, 11766 – 11775.
[4] L. Sun, R. M. Crooks, *J. Am. Chem. Soc.* **2000**, *122*, 12340 – 12345.
[5] E. Reimhult, K. Kumar, *Trends Biotechnol.* **2008**, *26*, 82 – 89.
[6] L. Song, M. R. Hobaugh, C. Shustak, S. Cheley, H. Bayley, J. E. Gouaux, *Science* **1996**, *274*, 1859 – 1866.
[7] H. Bayley, P. S. Cremer, *Nature* **2001**, *413*, 226 – 230.
[8] S. B. Lee, D. T. Mitchell, L. Trofin, T. K. Nevanen, H. Söderlund, C. R. Martin, *Science* **2002**, *296*, 2198 – 2200.
[9] C. Dekker, *Nat. Nanotechnol.* **2007**, *2*, 209 – 215.
[10] L. Zhao, M. Yosef, M. Steinhart, P. Göring, H. Hofmeister, U. Gösele, S. Schlecht, *Angew. Chem.* **2006**, *118*, 317 – 321; *Angew. Chem. Int. Ed.* **2006**, *45*, 311 – 315.
[11] C. C. Striemer, T. R. Gaborski, J. L. McGrath, P. M. Fauchet, *Nature* **2007**, *445*, 749 – 753.
[12] M. J. Kim, M. Wanunu, D. C. Bell, A. Meller, *Adv. Mater.* **2006**, *18*, 3149 – 3153.
[13] L. A. Baker, Y. S. Choi, C. R. Martin, *Curr. Nanosci.* **2006**, *2*, 243 – 255.
[14] P. Kohli, C. C. Harrell, Z. Cao, R. Gasparac, W. Tan, C. R. Martin, *Science* **2004**, *305*, 984 – 986.
[15] W. Lee, R. Ji, U. Gosele, K. Nielsch, *Nat. Mater.* **2006**, *5*, 741 – 747.
[16] W. Chen, J. S. Wu, X. H. Xia, *ACS Nano* **2008**, *2*, 959 – 965.
[17] H. Asoh, S. Ono, T. Hirose, M. Nakao, H. Masuda, *Electrochim. Acta* **2003**, *48*, 3171 – 3174.
[18] N. W. Liu, A. Datta, C. Y. Liu, Y. L. Wang, *Appl. Phys. Lett.* **2003**, *82*, 1281 – 1283.
[19] H. Masuda, H. Asoh, M. Watanabe, K. Nishio, M. Nakao, T. Tamamura, *Adv. Mater.* **2001**, *13*, 189 – 192.
[20] F. Matsumoto, K. Nishio, H. Masuda, *Adv. Mater.* **2004**, *16*, 2105 – 2108.
[21] T. Yamashita, S. Kodama, M. Ohto, E. Nakayama, N. Takayanagi, T. Kemmei, A. Yamaguchi, N. Teramae, Y. Saito, *Chem. Commun.* **2007**, 1160 – 1162.
[22] Q. Liu, Y. Wang, W. Guo, H. Ji, J. Xue, Q. Ouyang, *Phys. Rev. E* **2007**, *75*, 051201.
[23] P. Ramírez, S. Mafe, A. Alcaraz, J. Cervera, *J. Phys. Chem. B* **2003**, *107*, 13178 – 13187.
[24] Q. S. Pu, J. S. Yun, H. Temkin, S. R. Liu, *Nano Lett.* **2004**, *4*, 1099 – 1103.
[25] J. B. Heng, A. Aksimentiev, C. Ho, P. Marks, Y. V. Grinkova, S. Sligar, K. Schulten, G. Timp, *Biophys. J.* **2006**, *90*, 1098 – 1106.
[26] X. Hou, L. Jiang, *ACS Nano* **2009**, *3*, 3339 – 3342.
[27] X. Hou, H. Dong, D. Zhu, L. Jiang, *Small* **2010**, *6*, 361 – 365.
[28] L. Wen, X. Hou, Y. Tian, F. Q. Nie, Y. Song, J. Zhai, L. Jiang, *Adv. Mater.* **2010**, *22*, 1021 – 1024.
[29] X. Hou, W. Guo, F. Xia, F. Q. Nie, H. Dong, Y. Tian, L. Wen, L. Wang, L. Cao, Y. Yang, J. Xue, Y. Song, Y. Wang, D. Liu, L. Jiang, *J. Am. Chem. Soc.* **2009**, *131*, 7800 – 7805.
[30] J. H. Yuan, F. Y. He, D. C. Sun, X. H. Xia, *Chem. Mater.* **2004**, *16*, 1841 – 1844.
[31] W. Chen, J. S. Wu, J. H. Yuan, X. H. Xia, X. H. Lin, *J. Electroanal. Chem.* **2007**, *600*, 257 – 264.
[32] V. Srinivasan, W. I. Higuchi, *Int. J. Pharm.* **1990**, *60*, 133 – 138.
[33] a) J. King, Jr., and S. W. Benson, *J. Chem. Phys.* **1966**, *44*, 1007 – 1014; b) L. R. Snyder, *J. Phys. Chem.* **1968**, *72*, 489 – 494.
[34] W. Chen, J. H. Yuan, X. H. Xia, *Anal. Chem.* **2005**, *77*, 8102 – 8108.
[35] C. L. Rice, R. Whitehead, *J. Phys. Chem.* **1965**, *69*, 4017 – 4024.

